UNIVERSITÄT AUGSBURG
Universitätsbibliothek

OPEN ACCESS
OPUS AUGSBURG

Intracerebroventricular enzyme infusion corrects central nervous system pathology and dysfunction in a mouse model of metachromatic leukodystrophy

S. Stroobants, D. Gerlach, Frank Matthes, D. Hartmann, J. Fogh, V. Gieselmann, R. D'Hooge, U. Matzner

Angaben zur Veröffentlichung / Publication details:

Stroobants, S., D. Gerlach, Frank Matthes, D. Hartmann, J. Fogh, V. Gieselmann, R. D'Hooge, and U. Matzner. 2011. "Intracerebroventricular enzyme infusion corrects central nervous system pathology and dysfunction in a mouse model of metachromatic leukodystrophy." *Human Molecular Genetics* 20 (14): 2760–69. https://doi.org/10.1093/hmg/ddr175.

Nutzungsbedingungen / Terms of use:

licgercopyright

Dieses Dokument wird unter folgenden Bedingungen zur Verfügung gestellt: / This document is made available under these conditions:
Deutsches Urheberrecht
Weitere Informationen finden Sie unter: / For more information see:
https://www.uni-augsburg.de/de/organisation/bibliothek/publizieren-zitieren-archivieren/publiz/

Intracerebroventricular enzyme infusion corrects central nervous system pathology and dysfunction in a mouse model of metachromatic leukodystrophy

Stijn Stroobants[1,†], Debora Gerlach[2,†], Frank Matthes[2], Dieter Hartmann[3], Jens Fogh[4], Volkmar Gieselmann[2], Rudi D'Hooge[1] and Ulrich Matzner[2,*]

[1]Laboratory of Biological Psychology, Department of Psychology, University of Leuven, Tiensestraat 102, B-3000 Leuven, Belgium, [2]Institut für Biochemie und Molekularbiologie, Rheinische Friedrich-Wilhelms-Universität, Nussallee 11, D-53115 Bonn, Germany, [3]Anatomisches Institut, Rheinische Friedrich-Wilhelms-Universität, Nussallee 10, D-53115 Bonn, Germany and [4]Zymenex A/S, Roskildevej 12C, DK-3400 Hillerød, Denmark

Arylsulfatase A (ASA) catalyzes the desulfation of sulfatide, a major lipid component of myelin. Inherited functional deficiencies of ASA cause the lysosomal storage disease (LSD) metachromatic leukodystrophy (MLD), which is characterized by intralysosomal accumulation of sulfatide, progressive neurological symptoms and early death. Enzyme replacement therapy (ERT) using intravenous injection of active enzyme is a treatment option for many LSDs as exogenous lysosomal enzymes are delivered to lysosomes of patient's cells via receptor-mediated endocytosis. Efficient treatment of MLD and other LSDs with central nervous system (CNS) involvement is, however, hampered by the blood–brain barrier (BBB), which limits transfer of therapeutic enzymes from the circulation to the brain parenchyma. To bypass the BBB, we infused recombinant human ASA (rhASA) by implanted miniature pumps into the cerebrospinal fluid (CSF) of a conventional and a novel, genetically aggravated ASA knockout mouse model of MLD. rhASA continuously delivered to the lateral ventricle for 4 weeks penetrated the brain parenchyma and was targeted to the lysosomes of brain cells. Histological analysis revealed complete reversal of lysosomal storage in the infused hemisphere. rhASA concentrations and sulfatide clearance declined with increasing distance from the infusion site. Correction of the ataxic gait indicated reversal of central nervous system dysfunctions. The profound histopathological and functional improvements, the requirement of low enzyme doses and the absence of immunological side effects suggest intracerebroventricular ERT to be a promising treatment option for MLD and other LSDs with prevailing CNS disease.

INTRODUCTION

Myelin contains the sphingolipid 3-O-sulfogalactosylceramide (sulfatide) that has important functions in myelin maintenance and integrity (1). The catabolism of sulfatide involves its transport from the myelin sheath to the lysosomal compartment of the myelinating cell and its stepwise degradation by a series of acid hydrolases (2). The first hydrolytic step, removal of the sulfate group from the galactosyl moiety, is catalyzed by the lysosomal enzyme arylsulfatase A (ASA; E.C. 3.1.6.8.). A deficiency of ASA activity cannot be compensated and undegraded sulfatide accumulates in the lysosome leading to the fatal lysosomal storage disease (LSD) metachromatic leukodystrophy (MLD) (3). MLD is characterized by intralysosomal deposition of sulfatide in Schwann cells, oligodendrocytes, neurons and other cell types, progressive loss of myelin sheaths in the peripheral nervous system (PNS) and central nervous system (CNS) and early death due to deteriorating neurological functions. Effective treatment is not available to date.

Enzyme replacement therapy (ERT) has been proved successful in several LSDs (4). The rationale for ERT is that cells express endocytic receptors, including the mannose

*To whom correspondance should be addressed. Tel: +49 228735046; Fax: +49 228732416; Email: matzner@ibmb.uni-bonn.de
†S.S. and D.G. share first authorship.

Table 1. Mouse models of MLD and corresponding controls

Model	Conventional		Aggravated	
Immune status	Competent	Tolerant	Competent	Tolerant
ASA knockout	ASA−/−	ASA−/−	ASA−/−	ASA−/−
PLP-CST transgene	–	–	PLP-CST+/−	PLP-CST+/−
hASAc69s transgene	–	hASAc69s+/−	–	hASAc69s+/−
Reference	(7)	(8)	(9)	This study
Control mice	ASA+/−	ASA+/− hASAc69s+/−	–[a]	ASA+/− PLP-CST+/− hASAc69s+/−

[a]Immune-competent mice with aggravated phenotype were not used in this study.

6-phosphate/insulin-like growth factor II receptor, which transport extracellular lysosomal enzymes to the lysosome (5). Due to lysosomal delivery, an intravenously injected functional counterpart of the defective enzyme therefore supplies patient's cells with active enzyme and compensates their catabolic defect. Thus far ERT has been successfully used to treat, for example, Gaucher disease type I, Fabry disease, mucopolysaccharidosis types I, II and VI and Pompe disease (4). However, almost 20 years of preclinical and clinical research has failed to resolve the issue of blood–brain barrier (BBB) impermeability that impedes efficient transfer of therapeutic enzyme from the circulation to the brain parenchyma and prevents the improvement of CNS manifestations (6). Consequently, ERT is inefficient for the treatment of LSDs with prevailing CNS pathology that in fact includes the majority of presently known LSDs (e.g. Tay-Sachs, Niemann-Pick and Gaucher disease type II).

Several mouse models of MLD have been generated (Table 1). The conventional ASA knockout mice store sulfatide and the tissue distribution of storage is comparable with human patients (7). The mice, however, do not develop a leukodystrophy most likely because they do not accumulate amounts of sulfatide sufficient to cause demyelination. Conventional ASA knockout mice have been genetically tolerized to recombinant human ASA (rhASA) by transgenic expression of an enzymatically inactive human ASA variant (8). Thus, immune-competent and immune-tolerant strains of conventional ASA knockout mice are available. The conventional, immune-competent model was also genetically modified by a transgene overexpressing the sulfatide-synthesizing sulfotransferase and thus increasing the sulfatide load (9). The transgenic mice accumulate more sulfatide than the conventional model and demyelinate in the PNS and CNS when they approach 2 years of age. An immune-tolerant strain of these aggravated MLD mouse model was generated for the present study (see Materials and Methods).

Repeated intravenous injection of rhASA into conventional ASA knockout mice reduces sulfatide storage and improves the nervous system function in a dose-dependent manner (10,11). Notably and in contradiction to what was expected, intravenous ERT diminished sulfatide levels also in the brain and spinal cord to some extent. Sulfatide clearance from the brain required, however, high enzyme doses of $\geq$20 mg/kg, and brain effects were undetectable if lower doses of 4 mg/kg were used. Also in a recent phase I/II clinical trial in which children with late-infantile MLD were treated with rhASA doses of up to 2.5 mg/kg, no readily discernible effects of ERT on motor or cognitive function became apparent (12). To reduce the costs required for high-dose treatment and to improve therapeutic efficacy, several alternatives to conventional peripheral ERT are under investigation. We presently report preclinical experiments in which the BBB of mice was bypassed by continuous infusion of rhASA into the brain ventricles using miniature osmotic pumps. Compared with intravenous ERT, such intracerebroventricular (i.c.v.) ERT requires substantially less therapeutic enzyme to clear more sulfatide from brain.

RESULTS

Stability of rhASA

The osmotic pumps utilized in the present study are implanted single-use devices (Fig. 1A) with its usability limited by a short half-life of the infusate. To analyze the stability of rhASA in the pump system, the activity of the solution remaining in the pump reservoir at the end of the treatment period was remeasured. This analysis revealed a mean residual activity (in U/ml) of 69.7% of the initial activity after 4 weeks of treatment ($n = 22$; data not shown).

Pharmakokinetics of rhASA

rhASA was infused into conventional, immune-tolerant ASA knockout mice (for an overview about the different mouse models used in this study see Table 1). The tissue distribution of rhASA was analyzed by measuring the rhASA activity in different brain regions. To this end, the infused cerebral hemisphere, the contralateral cerebral hemisphere, the hind brain (cerebellum and brain stem), the cervical spinal cord and the thoracal spinal cord were separately analyzed. To differentiate between substituted rhASA, endogenous hASAc69s and unspecific sulfatases, rhASA was immunoprecipitated from tissue homogenates and the sulfatase activity of the precipitate was measured. This analysis revealed rhASA levels decreasing from the ipsi- to the contralateral hemisphere and along the rostro-caudal axis of the CNS (Fig. 1B). ASA activity was undetectable in the cervical spinal cord, thoracal spinal cord, kidney and serum (not shown in Fig. 1B).

To estimate the tissue half-life of rhASA, the rhASA level of the total brain was related to the amount of infused enzyme determined by the difference between the start and

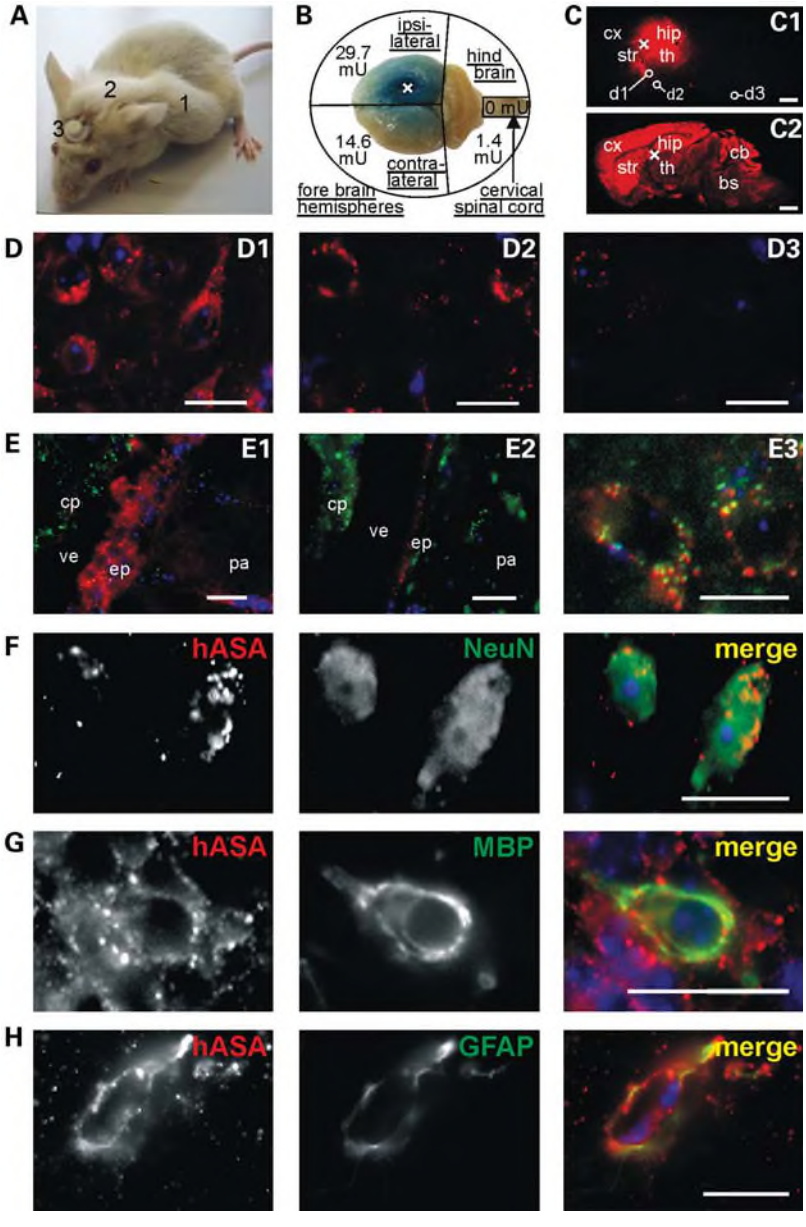

Figure 1. Distribution of rhASA. (**A**) Mouse with implanted miniature pump (1) delivering rhASA through a catheter (2) to the i.c.v. cannula fixed with a pedestal (3) on the cranial bone. (**B**) Mean rhASA levels in the indicated regions of $n = 7$ conventional, immune-tolerant ASA knockout mice after i.c.v. infusion of 1 mg/ml rhASA for 4 weeks. The dissected brain shown in the top view is from an independent experiment in which 0.5 mg/ml Evans blue was infused to visualize the dissemination of a tracer delivered by the pump system. cross, infusion site. (**C**) Immunostaining of rhASA (red) in parasagittal brain sections through the injection site (cross) of a conventional, immune-competent ASA knockout mouse treated with rhASA (C1) and, as a positive control, a mock-treated conventional, immune-tolerant ASA knockout mouse (C2). bs, brain stem; cb, cerebellum; cx, cerebral cortex; hip, hippocampus; str, striatum; th, thalamus. Sections from the circled areas D1–D3 are shown under higher magnification in (D). Bars represent 1.3 mm. (**D**) Higher magnification of areas depicted in C1 showing the subcellular localization of rhASA (red). (**E**) Co-immunostaining of rhASA (red) and Lamp-2 (green). The ependyma of the injected lateral ventricle (E1), the ependyma of the fourth ventricle (E2) and striatum cells with neuronal morphology (E3) are shown. cp, choroid plexus; ep, ependyma; pa, parenchyma; ve, ventricle. (**F**) Co-immunostaining of rhASA and the neuronal marker NeuN. (**G**) Co-immunostaining of rhASA and the oligodendroglial marker MBP. (**H**) Co-immunostaining of rhASA and the astroglial marker GFAP. Bars in (D)–(H) represent 20 μm.

end volumes of the infusate. This calculation indicated a rhASA recovery of 0.9%, suggesting a mean rhASA tissue half-life of <10 min. To verify this unexpected low half-life, rhASA levels of conventional, immune-competent ASA knockout mice treated with 1 mg/ml rhASA were measured by a human ASA-specific enzyme-linked immunosorbent assay (ELISA). This analysis is not possible in immune-tolerant ASA knockout mice due to cross-reacting endogenous hASAc69s. Again, $<1\%$ of the infused rhASA could be retrieved by this ELISA (data not shown).

To investigate the distribution of rhASA by immunohistochemistry, rhASA was infused into the brain of conventional, immune-competent ASA-deficient mice (Table 1) in a separate set of experiments. The cellular and subcellular distribution of infused rhASA was analyzed by immunostaining of sagittal brain sections with anti-hASA antibodies. Under

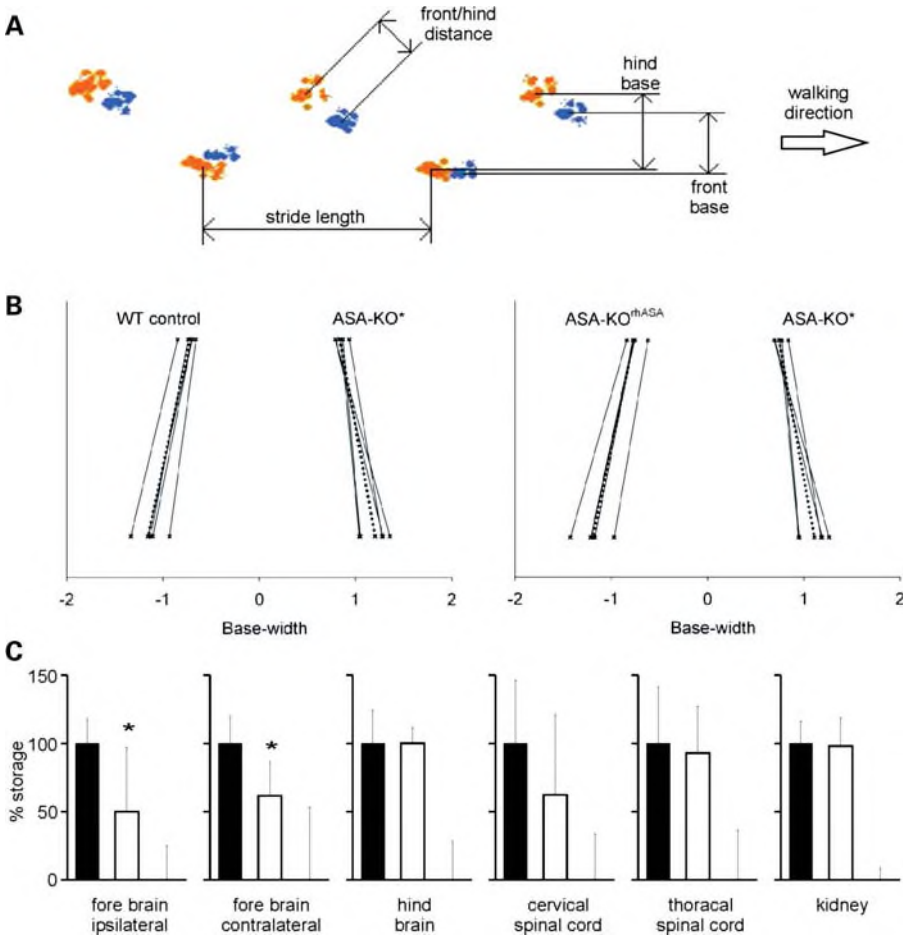

Figure 2. Corrective effects of i.c.v. ERT on gait alterations and sulfatide storage of conventional, immune-tolerant ASA knockout mice. (**A**) Paw print profile illustrating the gait parameters measured via treadmill gait analysis. Fore paws are painted in blue, hind paws in orange. Parameters shown: front base, distance between the front paws; hind base, distance between the hind paws; front/hind distance (left–right), distance between placement of the front paw and the subsequent placement of the ipsilateral hind paw; stride length (for each paw), distance between two subsequent placements of the same paw. (**B**) Unilateral print vectors illustrate differences in front versus hind base congruity for wild-type control mice ($n = 5$; left panel) in comparison with mock-treated conventional, immune-tolerant ASA knockout mice ($n = 5$; both panels right). Front and hind paw prints are connected through vector lines. Dotted and solid lines represent group means and individual scores, respectively. There is a strong relationship between the front base and hind base in wild-type control mice, resulting in an approximately parallel set of print vectors. In contrast, a high level of incongruity for these parameters exists in conventional, immune-tolerant ASA knockout mice (left panel). Notably, this lack of uniformity was completely reversed after i.c.v. treatment (right panel). (**C**) Sulfatide levels in the indicated regions of the CNS and in kidneys were analyzed by TLC, normalized on cholesterol levels and compared between mock-treated ASA knockout mice (closed bar), rhASA-treated ASA knockout mice (open bar) and wild-type controls (whiskers only). Bars represent means $\pm$ SDs of $n = 7–8$ animals per group. Asterisks indicate a significant difference between rhASA- and mock-treated ASA knockout mice ($P < 0.05$).

low magnification, rhASA was readily detectable in the parenchyma of the ipsilateral cerebral hemisphere demonstrating that rhASA efficiently crosses the ependyma of the lateral ventricle and distributes in the brain tissue (Fig. 1C). Higher magnification confirmed transfer of rhASA into the brain parenchyma (Fig. 1D), but also showed considerable accumulation of enzyme in the ependymal cell layer (Fig. 1E1 and E2). Notably, rhASA was also detectable in large distances from the infusion site, such as the brain stem (Fig. 1D3). In the brain parenchyma, rhASA was efficiently endocytosed (Fig. 1D). Delivery to the endosomal/lysosomal compartment was verified by costaining of LAMP-2 (Fig. 1E3). Costaining of NeuN, myelin basic protein (MBP) or glial fibrillary acidic protein (GFAP) indicated uptake of rhASA by neuronal, oligodendroglial and astroglial cells (Fig. 1F–H).

Normalization of the ataxic gait

Pumps continuously delivering 1 mg/ml rhASA into the right lateral ventricle were implanted into 6-month-old conventional, immune-tolerant ASA knockout mice. Various behavioral parameters were analyzed in the second to fourth week of treatment. Control groups were age-matched immune-tolerant ASA knockout mice and wild-type controls that were implanted with pumps delivering vehicle. No differences between groups were found for swimming velocity or treadmill performance (data not shown). Gait analysis revealed, however, significant differences between mock-treated ASA knockout mice and wild-type controls which reflect the previously reported motor incoordination and reduced gait homogeny of ASA knockout mice (Fig. 2A and B, Table 2) (13). Specifically, the front/hind distances and incongruity

Table 2. Normalization of gait parameters by i.c.v. ERT of ASA knockout mice

Group treatment	Wild-type control vehicle	ASA knockout vehicle	ASA knockout rhASA
Front base width[a] (cm)	1.59	1.48	1.59
Hind base width (cm)	2.35	2.47	2.38
Left front-hind distance (cm)	1.60	**1.90**$^{**,+}$	1.73
Right front-hind distance (cm)	1.63	**2.10**$^{***,+++}$	1.73
Left front stride length (cm)	4.79	5.11	**5.16***
Right front stride length (cm)	4.94	5.29	5.26
Left hind stride length (cm)	4.92	5.31	5.31
Right hind stride length (cm)	4.76	5.14	**5.29****
IC[b] (front to hind base)	0.49	**1.24**$^{***,++}$	0.58
IC (front to hind stride length)	0.09	**0.30**$^{***,+++}$	0.08
IC (left to right stride length)	0.05	**0.17**$^{**,+}$	0.09

[a]The indicated gait parameters are illustrated in Figure 2A.
[b]IC, incongruity coefficient.
Stars and bold letters indicate a statistically significant difference to wild-type controls: $^{***}P < 0.001$, $^{**}P < 0.01$, $^{*}P < 0.05$. Plus signs and gray bars indicate a statistically significant difference between vehicle- and rhASA-treated ASA knockout mice: $^{+++}P < 0.001$, $^{++}P < 0.01$, $^{+}P < 0.05$. Values are means of $n = 10–12$ mice per group.

coefficients for base widths and stride lengths were significantly increased in ASA knockout mice. Previous analyses of 6-month-old ASA knockout mice revealed an increased hind base width and increased stride lengths (13), but these findings were only partially confirmed in the present study. Notably, continuous i.c.v. infusion of rhASA reversed all ataxic features except the stride length changes (Table 2). Front/hind distances and incongruity coefficients were significantly decreased to a level indistinguishable from wild-type mice and hind and front base widths diminished to near wild-type values. Beneficial effects of i.c.v. treatment on front versus hind base incongruity in ASA knockout mice are illustrated in Figure 2B.

Sulfatide reduction in different CNS regions

Sulfatide levels in the CNS of conventional, immune-tolerant ASA knockout mice were examined 4 weeks after pump implantation. For biochemical analysis of storage, different regions of the CNS were separately analyzed by thin layer chromatography (TLC). This comparison revealed a significant decline of sulfatide storage in the infused cerebral hemisphere of rhASA-treated MLD mice by 51.4% ($P = 0.008$) and in the contralateral cerebral hemisphere by 38.2% ($P = 0.003$) (Fig. 2C). The extent of sulfatide reduction was comparable in the cervical spinal cord (37.3%), but only borderline significant due to the higher variability of values ($P = 0.089$). Sulfatide levels were virtually unchanged in the hind brain (cerebellum and brain stem; 0.6% less, $P = 0.475$), the thoracal spinal cord (4.8% less, $P = 0.414$) and in kidney that was analyzed as a negative tissue control (2.4% less, $P = 0.408$).

In the histological analysis, sulfatide storage, which occurred as intense alcianophilia, was visible in the fimbria, corpus callosum, capsula interna (data not shown), brain stem and cervical spinal cord of mock-treated ASA knockout mice (Fig. 3A). As described previously, different types of alcianophilic profiles can be morphologically distinguished and attributed to different cell types (10): (i) bizarre-shaped, compact profiles >20 μm typical for phagocytes (indicated in Fig. 3A, pontine reticular nucleus, by closed arrow heads), (ii) ring-shaped, disconnected profiles >20 μm characteristic of neuronal perikarya (indicated in Fig. 3A, pontine reticular nucleus, by open arrow heads), (iii) small profiles <5 μm typical for oligodendrocytes and possibly other cell types with low storage (visible, for example, in Fig. 3A, fimbria of the mock-treated mouse). Alcianophilic material was undetectable in wild-type controls (data not shown). Treatment caused almost complete disappearance of alcianophilic material from the infused and contralateral cerebral hemisphere, marked reduction in the brain stem and some decline in the white matter of the cervical spinal cord (Fig. 3A). In contrast, there was no sulfatide clearance from the gray matter of the spinal cord.

Sulfatide reduction in an aggravated MLD mouse model

To determine the extent of sulfatide reduction in a mouse model that reproduces a more MLD-like phenotype with increased sulfatide storage, 6-month-old immune-tolerant ASA knockout mice overexpressing cerebroside sulfotransferase (Table 1) were treated with 1 mg/ml rhASA for 4 weeks. As seen for mock-treated animals in Figure 3, sulfatide storage of the aggravated mouse model is substantially amplified in various regions of the brain compared with conventional ASA knockout mice. The histological picture is particularly dominated by massive storage of brain phagocytes. However, small alcianophilic profiles typical of oligodendrocytes are also more abundant. Histological analysis of rhASA-treated mice showed a virtually complete clearance of all types of alcianophilic storage material from the ipsilateral hemisphere (Fig. 3B). In the contralateral hemisphere, storage patterns typical for phagocytes are no longer detectable, while storage profiles characteristic of oligodendrocytes persist. Cell type-specific differences are also seen in the pontine reticular nucleus of the brain stem where storage of phagocytes is reduced, whereas neuronal storage is unchanged. Similar to conventional ASA knockout mice, storage is diminished in white but not gray matter of the cervical spinal cord. TLC of lipid extracts from different CNS tissues revealed that i.c.v. ERT reduced sulfatide storage in the infused hemisphere, the contralateral hemisphere, cervical spinal cord and hind brain by 55.9% ($P = 0.0004$), 27.3% ($P = 0.045$), 12.7% ($P = 0.190$) and 8.0% ($P = 0.297$), respectively (means of $n = 7$ mice per group; data not shown).

Adverse effects of i.c.v. infusion

The total body weight declined post-surgery to a similar extent in rhASA-treated mice and controls, indicating that i.c.v. ERT with rhASA has no additional adverse effect (data not shown). This weight loss seemed to be due to reduced food intake shortly after surgery as mice regained their normal weight during the course of the experiment. Also the brain wet weights determined after 4 weeks of treatment were undistinguishable between the groups (data not shown). To detect a possible humoral immune response to substituted rhASA, anti-

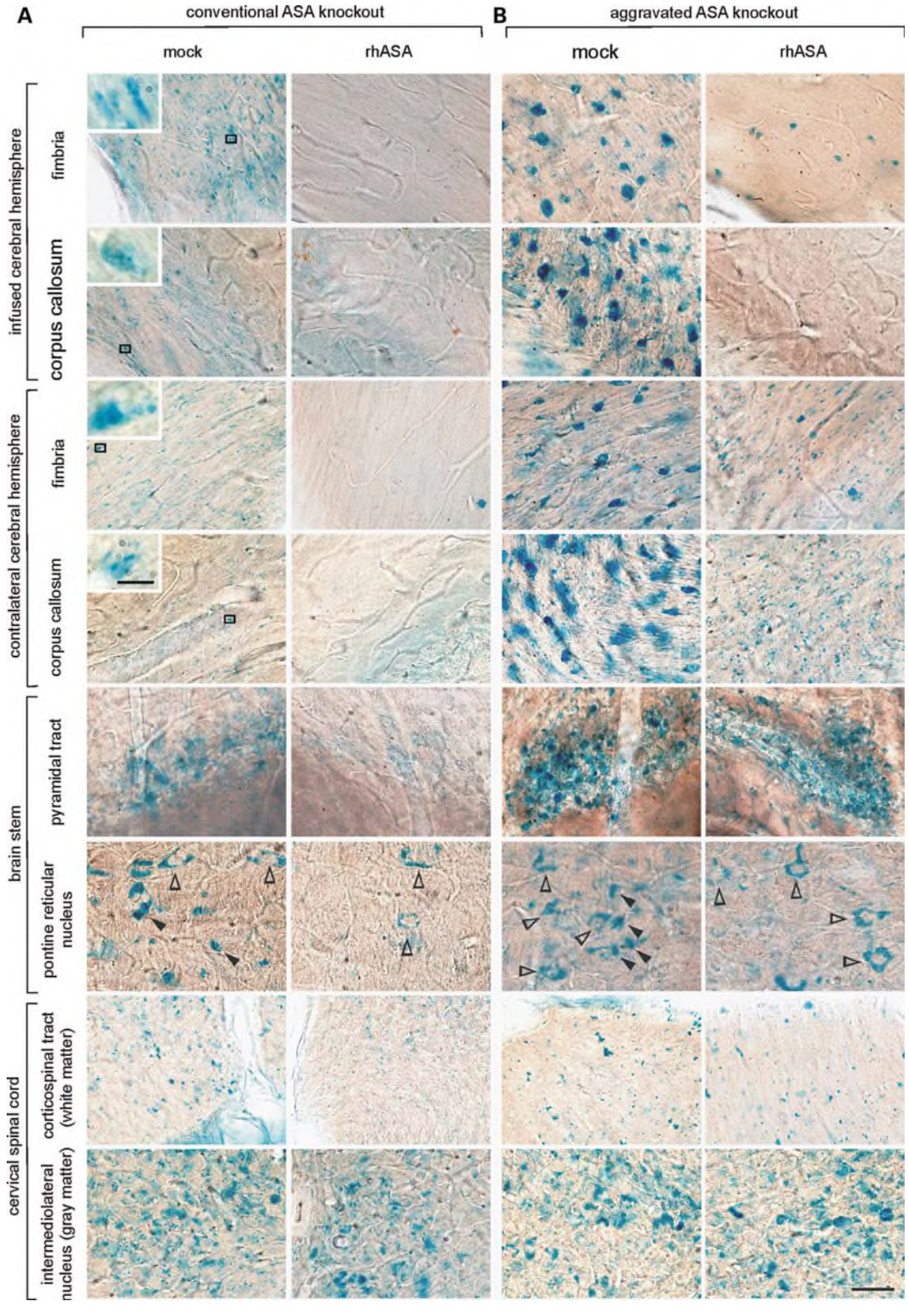

Figure 3. Sulfatide storage in the CNS of mock- and rhASA-treated immune-tolerant ASA knockout mice of the conventional (**A**) and aggravated phenotype (**B**), respectively. Compared are different regions of the brain and spinal cord as indicated on the left. Sections were stained with the cationic dye alcian blue. No alcianophilic material was detectable in corresponding sections of wild-type control mice (data not shown). Inserts in (A) are higher power images of boxed areas to reveal storage in fimbria and corpus callosum of mock-treated conventional ASA knockout mice which are hard to see in the overview images. For the pontine reticular nucleus of the brain stem, the morphologically distinct storage patterns of phagocytes and neurons are indicated by closed and open arrow heads, respectively (for details see text). Representative sections from $n = 3$ mice per experimental group are shown. Bars represent 50 μm (overview images) and 5 μm (inserts), respectively.

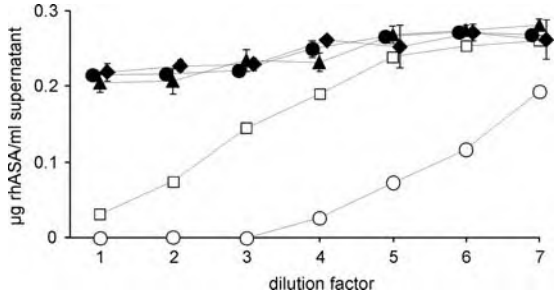

Figure 4. Anti-rhASA antibodies in serum. For the determination of the antibody titer, serial 1-to-1 dilutions of mouse serum were incubated with a fixed amount of rhASA and immune complexes were precipitated. The residual ASA concentration of the supernatant is a measure for the level of anti-rhASA antibodies in the respective serum dilution. Antibodies were readily detectable in two immune-competent control animals which had received four repeated intravenous injections of rhASA (open circle: rabbit, 4× 100 µg; open squares: ASA knockout mouse, 4× 600 µg) (15). Antibodies were undetectable in conventional, immune-competent ASA knockout mice treated by i.c.v. ERT (closed triangles, $n = 6$). Antibodies were also absent from conventional, immune-tolerant ASA knockout mice, treated as a negative control, either by i.c.v. infusion of rhASA (closed circles, $n = 3$) or buffer (closed diamonds, $n = 3$). Data points and bars shown for the latter three groups represent means ± SDs of $n = 3–6$ animals.

rhASA antibodies were titered in serum of conventional, immune-competent ASA knockout mice and, as a negative control, in serum of conventional, immune-tolerant ASA knockout mice, both treated by i.c.v. ERT. In neither of the two groups, antibodies to rhASA were detectable (Fig. 4). In contrast, antibodies were readily detectable in sera of immune-competent animals treated by intravenous ERT as a positive control.

DISCUSSION

The main limitation of intravenous ERT for the treatment of LSDs with primary neurological involvement is the inability of peripherally introduced therapeutic enzyme to cross the BBB efficiently (6). Experiments in animal models of mucopolysaccharidosis types I, II and IIIA have shown that enzyme delivered via the intrathecal route distributes throughout the CNS and promotes widespread clearance of lysosomal storage material (14). In the present study, we tested the potential of i.c.v. ERT to improve the brain pathology of MLD mouse models. Treatment was initiated at 6 months, an age at which gait alterations become detectable in ASA knockout mice (13). This stage was chosen because the onset of gait disturbances is usually regarded to be pathognomonic for late-infantile MLD and defines the starting point for intervention in the clinical situation (3).

After infusion of rhASA into the right lateral ventricle, immunostaining of brain sections and ASA activity measurements in different brain regions show widespread distribution of rhASA with levels decreasing from the ipsi- to the contralateral hemisphere and along the rostro-caudal axis (Fig. 1B–D). Apparently, rhASA penetrates the ependymal cell layer and distributes throughout the brain parenchyma, reaching regions quite distant from the infusion site (Fig. 1D3). Furthermore, as shown for neurons, oligodendrocytes and astrocytes rhASA is rapidly taken up by brain cells (Fig. 1F–H). Colocalization of rhASA and Lamp-2 indicates lysosomal sorting of endocytosed enzyme (Fig. 1E3), probably due to mannose 6-phosphate-dependent targeting (15–17). As shown by biochemical and histological analysis of sulfatide storage, lysosomal delivery of substituted rhASA causes a correction of the catatabolic defect (Figs 2C and 3). The extent of sulfatide clearance seems to depend on local rhASA tissue concentrations, but also on the cell type. Cell type-specific differences are most clearly visible in a novel optimized MLD mouse model that, due to three independent genetic modifications, is ASA-deficient, expresses an inactive ASA variant and displays increased sulfatide synthesis. Due to the presence of cross-reacting immunological material and increased lysosomal storage which causes reduced nerve conduction velocity and severe neurological symptoms in the second year of age, this model closely mimicks the pathological features of MLD patients (9). As seen in different CNS regions of this mouse model, phagocytes seem to be most responsive to treatment as their storage disappears also in regions distant from the infusion site, such as the brain stem (Fig. 3B). Storage of oligodendrocytes, on the other hand, is abrogated in the infused hemisphere but still present in the contralateral hemisphere, indicating the requirement of higher rhASA concentrations for correction in this cell type. Neurons are also more resistant to treatment since neuronal storage appears to be unchanged in the pontine reticular nucleus of the brain stem, although phagocytes are corrected. The dose-dependent and cell type-specific clearance of sulfatide clearly points to the requirement of higher enzyme doses potentially delivered by bilateral pumps to improve therapeutic efficacy of i.c.v. ERT.

Another strategy to improve the therapeutic efficacy might be to increase the short half-life of the infused rhASA which was found to be <10 min. This was surprising as the tissue half-life of rhASA administered via the intravenous route ranges between 3 and 4 days (10). The discrepancy might be partially ascribed to the bulk flow of the cerebrospinal fluid (CSF) which is produced by the choroid plexus and circulates from the lateral ventricles to the subarachnoid space of the brain and the spinal cord where it is reabsorbed into the blood via arachnoid granulations. The CSF volume and production rate in the mouse is 35 µl and 18 µl/h, respectively (18). This means that the elimination half-life for any compound which is not retained within the brain, e.g. by cellular uptake, is ∼1 h. The brain half-life of rhASA is, however, even lower than 1 h, indicating that additional processes such as protein degradation contribute to the rapid loss of enzyme. In terms of bioavailability and therapeutic benefit, methods to stabilize rhASA in the CSF and/or brain parenchyma would, therefore, be highly advantageous.

In a previous preclinical study using intravenous ERT, 52 rhASA injections of 50 mg/kg, resembling a cumulative dose of ∼86 mg per mouse, were required to reduce brain sulfatide storage by 34% (11), whereas in the present study a mere 120 µg of rhASA diminished sulfatide storage in the infused hemisphere by 51–56%. Thus, <0.2% of the intravenous dose was more effective in the CNS when administered i.c.v. Moreover, ASA knockout mice that are not tolerized to human ASA do not express antibodies to rhASA delivered to the CSF (Fig. 4), whereas the same mice develop lethal

anaphylactic reactions and/or resistance to treatment during 4 weeks of repeated intravenous ERT (Fig. 4) (10,15). It has to be mentioned that, contrary to our data for the MLD mouse model, i.c.v. ERT induced a profound humoral immune response in a mouse model and two dog models of other LSDs (19–21). These models were, however, not treated by implanted pumps delivering enzyme to the lateral ventricle, but by repeated bolus injection of comparably high enzyme doses into the cerebellomedullary cistern. The different outcome might therefore be ascribed to differences in the application mode and/or cumulative enzyme dose. Alternately, as many LSDs also affect immune cells, still unrecognized and disease-specific irregularities in the function of the immune system may exist (22).

The most important finding of the present study is the marked improvement of nervous system function. As already shown in previous studies (13,23), 6-month-old ASA knockout mice show different changes reflecting motor incoordination and gait asynchrony (Table 2, Fig. 2B). Remarkably, i.c.v. ERT completely reverses most of these ataxic features. Thus, treatment significantly decreases front/hind distances and incongruity coefficients for base widths and stride lengths to a level indistinguishable from wild-type mice. On the other hand, increased stride lengths typical for ASA knockout mice of that age do not change. It is important to note that this parameter was completely normalized by intravenous ERT with low doses of 4 mg/kg rhASA, a regimen that was proved to be successful in correcting storage in the PNS but not the CNS (10). These findings suggest that increased stride lengths in ASA knockout mice are the consequence of PNS dysfunction and are therefore unlikely to benefit from the present treatment protocol which targets specifically CNS pathology and dysfunction. Consequently, a combination therapy that combines i.c.v. and intravenous ERT is likely to correct all aspects of gait deterioration. Gait changes which eventually evolve into severe ataxia in MLD mice were predominantly ascribed to the development of pronounced cerebellar pathology (13,23). However, in the present study, we have shown that i.c.v. ERT reverses gait alterations in these mice at the age of 6 months in the absence of substantial sulfatide reduction in the cerebellum (Fig. 2C, hind brain). Furthermore, storage reduction in the spinal cord was more pronounced following intravenous ERT, which resulted in more modest motor improvements (11). These findings suggest that initial gait alterations in MLD mice (and patients) could have a frontal origin, as storage reduction following i.c.v. ERT declines along the rostro-caudal axis. Notably, ASA knockout mice accumulate sulfatide in the pallidum and the subthalamic nucleus in concordance with storage patterns of human patients (24). Early changes in gait due to basal ganglia dysfunctions might therefore precede the severe ataxia that likely results from multistructural damage.

In summary, the present study demonstrates that, in contrast to intravenous ERT, i.c.v. ERT reverses previously intractable ataxic symptoms of MLD, requires less enzyme to clear more sulfatide from brain and has no adverse immunological effects. Implantable pump systems for drug delivery to the CSF are routinely used in various clinical conditions, for example, opioid or baclofen administration in patients with chronic pain and spasticity, respectively (25). The demonstrated therapeutic efficacy in MLD mouse models and the well-established clinical feasibility with miniaturized pump systems suggest that i.c.v. ERT could be a promising option for future treatment of MLD and other LSDs with CNS manifestations.

MATERIALS AND METHODS

Recombinant human ASA

rhASA was produced in stably transfected Chinese hamster ovary cells under bioreactor conditions and purified from the medium by combinations of ion-exchange and hydrophobic chromatography (for details see http://www.freepatentsonline.com/y2008/0003211.html).

Experimental animals

Three mouse models of MLD were used in this study: immune-competent conventional ASA knockout mice (7), immune-tolerant conventional ASA knockout mice (8) and immune-tolerant ASA knockout mice with aggravated phenotype (Table 1). The latter strain is a novel MLD mouse model which was generated by crossbreeding of hASAc69s transgenic ASA knockout mice (8) with ASA knockout mice overexpressing cerebroside sulfotransferase (CST) from the proteolipid protein (PLP) gene promoter (9). The resulting double-transgenic ASA knockout mice combine the phenotypical features of their parental strains, immune tolerance to human ASA and an aggravated MLD-like storage phenotype (Fig. 3B). Control mice were age-matched litter mates being heterozygous for the ASA null allele and the transgenes of the corresponding knockout strain (Table 1). The controls are designated as ‘wild-type’ controls for reasons of simplicity. Mice had the mixed genetic background 129ola × C75BL/6 and were kept under standard housing conditions in accordance with the current German law on the protection of animals. All animal experiments were approved by the local committee for animal welfare (LANUV reference number 87-51.04.2010.A186).

Treatment of mice

The osmotic miniature pump model 2004 and the brain infusion kit 3 from Alzet (Cupertino, CA, USA) were implanted according to the manufacturer’s recommendations. Briefly, mice were anesthetized by intraperitoneal injection of 5% chloral hydrate (1% of body weight). Cannulas were stereotactically implanted into the right lateral ventricle using the coordinates obtained from Paxinos and Franklin (26): 1 mm posterior to bregma, 1 mm lateral to midline and 2 mm from skull surface. Each pump was filled with 200 μl of rhASA (1 mg/ml). A catheter tube was used to connect the cannula with the osmotic pump which was subcutaneously implanted into the back of the mouse. At termination, mice were deeply anesthetized, the pump was excised and the residual volume of the rhASA solution was measured. A volume of 120.9 ± 11.1 μl (mean ± SD; $n = 63$) was infused during a treatment period of 4 weeks.

Biochemical analysis

Anesthetized mice were transcardially perfused with 1× PBS pH 7.4 and the brain, spinal cord and kidneys were dissected. Tissue samples were homogenized in tris buffered saline (1× TBS) pH 7.4 for lipid extraction (10), protein determination (BioRad Dc assay, BioRad, Hercules, CA, USA), measurements of ASA by ELISA (27) and activity assays. For activity assays, rhASA was quantitatively immunoprecipitated from the homogenate with the non-inhibiting mouse anti-hASA antibody 19-16-3 (15,28) and Pansorbin cells (Calbiochem-Novabiochem, La Jolla, CA, USA). The ASA activity of the precipitate was measured with the chromogenic substrate para-nitrocatechol sulfate (29). Lipids were analyzed by TLC (10). Sulfatide levels were normalized on cholesterol levels and the sulfatide/cholesterol ratios of different experimental groups were compared. Percentage of storage reduction refers to the difference between mock-treated ASA knockout mice and mock-treated wild-type animals, which was regarded as 100%. Antibody titers were determined by measuring the capacity of serum to immunoprecipitate rhASA (15).

Histology

Brain and spinal cord were dissected from mice fixed by transcardial perfusion of 4% (w/v) paraformaldehyde in 1× PBS pH 7.4 and 6% (v/v) glutaraldehyde in 0.1 M sodium phosphate buffer pH 7.4, respectively. For the detection of sulfatides, vibratome sections (100 μm thick) prepared from glutaraldehyde-fixed tissues with a Leica VT 1200S (Leica Microsystems, Wetzlar, Germany) were incubated with alcian blue (24,30). For immunostaining, cryosections (10 μm thick) from paraformaldehyde-fixed tissues were prepared with a Leica CM 3050 (Leica Microsystems), stained as described (17) and analyzed by epifluorescence microscopy using an Axioskop 2 mot (Zeiss, Jena, Germany) and a FLA-5100 fluorescence scanner (Fujifilm Life Science, Tokyo, Japan), respectively. Affinity-purified rabbit anti-hASA antiserum (28), rat anti-Lamp-2 antibody ABL-93 (DSHB, Iowa, USA), rat anti-MBP antibody (Abcam, Cambridge, USA), mouse anti-NeuN antibody (Millipore, Schwalbach, Germany) and mouse anti-GFAP antibody (ICN Pharmaceuticals, Frankfurt, Germany) were used as primary antibodies and diluted 1:100. Secondary antibodies were Cy3-conjugated goat anti-rabbit IgG antibody (1:800; Dianova, Hamburg, Germany), DyLight 488-conjugated goat anti-rat IgG antibody (1:800; Dianova) and MFP488-conjugated goat anti-mouse IgG antibody (1:100; MoBiTec, Goettingen, Germany).

Behavioral tests

Swimming velocity, treadmill endurance and gait were analyzed basically as described (11). For the determination of gait parameters, mice were placed on a transparent treadmill belt and confined to the belt surface via a plexiglass cuboid (39.5 × 7.2 × 5.5 cm; video area 13 × 5.2 cm). Following a 30 s habituation trial, mice were tested for 60 s at a constant speed of 22 cm/s. Mice were encouraged to keep pace with the motor-driven treadmill using an electric grid placed at the end of the treadmill (0.8 mA). Treadmill performance in terms of error latency and number of errors were recorded. Ventral mirror-reflected imagery was captured with a USB webcam (resolution 640 × 480 pixels; 30 Hz) mounted 12 cm sideways from the belt. Several basic gait parameters were extracted from these video data using an automated algorithm: base widths (distance between contralateral paw prints), front/hind distances (distance between front paw print and subsequent hind paw print) and stride lengths (distance between subsequent prints of the same paw). Additionally, coefficients of incongruity were calculated as a measure of gait uniformity. These coefficients are defined as the absolute value of the difference between the standard scores or *z*-scores for the subject on two concurrent parameters. Dissimilar deviations of the group mean for the parameters will result in a higher score for incongruity.

Statistics

For the evaluation of biochemical data, statistical analysis was done by unpaired Student's *t*-test using InStat version 3.06 (GraphPad, San Diego, CA, USA). $P < 0.05$ was considered statistically significant. For behavioral tests, group comparisons were carried out using analysis of variance (ANOVA) procedures with Fisher LSD tests for *post hoc* analysis. The significance threshold was set at $\alpha = 0.05$.

ACKNOWLEDGEMENTS

We thank Renate Lüllmann-Rauch (Kiel, Germany) and Matthias Eckhardt (Bonn, Germany) for help with the histological analysis and for providing mice transgenic for cerebroside sulfotransferase, respectively. We thank Birgit Rau and Angelika Zoons for excellent technical assistance.

Conflict of Interest statement. None declared.

FUNDING

This work was supported by the two grants from the Seventh Framework Programme for research, technological development and demonstration activities of the European Community *LeukoTreat* (grant number 241622 to V.G.) and *Alpha-Man* (grant number 261331 to R.D'H.).

REFERENCES

1. Eckhardt, M. (2008) The role and metabolism of sulfatide in the nervous system. *Mol. Neurobiol.*, **37**, 93–103.
2. Kolter, T. and Sandhoff, K. (2005) Principles of lysosomal membrane digestion: stimulation of sphingolipid degradation by sphingolipid activator proteins and anionic lysosomal lipids. *Annu. Rev. Cell Dev. Biol.*, **21**, 81–103.
3. von Figura, K., Gieselmann, V. and Jaeken, J. (2001) Metachromatic leukodystrophy. In Scriver, C.R., Beaudet, A.L., Sly, W.S., Valle, D., Childs, B., Kinzler, K.W. and Vogelstein, B. (eds). *The Metabolic and Molecular Bases of Inherited Disease*. McGraw-Hill, New York, pp. 3695–3724.
4. Beck, M. (2010) Therapy for lysosomal storage disorders. *IUBMB Life*, **62**, 33–40.
5. Braulke, T. and Bonifacino, J.S. (2009) Sorting of lysosomal proteins. *Biochim. Biophys. Acta*, **1793**, 605–614.

6. Begley, D.J., Pontikis, C.C. and Scarpa, M. (2008) Lysosomal storage diseases and the blood-brain barrier. *Curr. Pharm. Des.*, **14**, 1566–1580.
7. Hess, B., Saftig, P., Hartmann, D., Coenen, R., Lüllmann-Rauch, R., Goebel, H.H., Evers, M., von Figura, K., D'Hooge, R., Nagels, G. *et al.* (1996) Phenotype of arylsulfatase A-deficient mice: relationship to human metachromatic leukodystrophy. *Proc. Natl Acad. Sci. USA*, **93**, 14821–14826.
8. Matzner, U., Matthes, F., Herbst, E., Lüllmann-Rauch, R., Callaerts-Vegh, Z., D'Hooge, R., Weigelt, C., Eistrup, C., Fogh, J. and Gieselmann, V. (2007) Induction of tolerance to human arylsulfatase A in a mouse model of metachromatic leukodystrophy. *Mol. Med.*, **13**, 471–479.
9. Ramakrishnan, H., Hedayati, K.K., Lüllmann-Rauch, R., Wessig, C., Fewou, S.N., Maier, H., Goebel, H.H., Gieselmann, V. and Eckhardt, M. (2007) Increasing sulfatide synthesis in myelin-forming cells of arylsulfatase A-deficient mice causes demyelination and neurological symptoms reminiscent of human metachromatic leukodystrophy. *J. Neurosci.*, **27**, 9482–9490.
10. Matzner, U., Herbst, E., Hedayati, K.K., Lüllmann-Rauch, R., Wessig, C., Schröder, S., Eistrup, C., Möller, C., Fogh, J. and Gieselmann, V. (2005) Enzyme replacement improves nervous system pathology and function in a mouse model for metachromatic leukodystrophy. *Hum. Mol. Genet.*, **14**, 1139–1152.
11. Matzner, U., Lüllmann-Rauch, R., Stroobants, S., Andersson, C., Weigelt, C., Eistrup, C., Fogh, J., D'Hooge, R. and Gieselmann, V. (2009) Enzyme replacement improves ataxic gait and central nervous system histopathology in a mouse model of metachromatic leukodystrophy. *Mol. Ther.*, **17**, 600–606.
12. i Dali, C. and Lund, A.M. (2009) Intravenous enzyme replacement therapy for metachromatic leukodystrophy (MLD). *ACMG Meeting*. March 25, Tampa, USA [abstracts].
13. Stroobants, S., Leroy, T., Eckhardt, M., Aerts, J.M., Berckmans, D. and D'Hooge, R. (2008) Early signs of neurolipidosis-related behavioural alterations in a murine model of metachromatic leukodystrophy. *Behav. Brain Res.*, **189**, 306–316.
14. Dickson, P.I. (2009) Novel treatments and future perspectives: outcomes of intrathecal drug delivery. *Int. J. Clin. Pharmacol. Ther.*, **47**(Suppl. 1), S124–S127.
15. Matzner, U., Matthes, F., Weigelt, C., Andersson, C., Eistrup, C., Fogh, J. and Gieselmann, V. (2008) Non-inhibitory antibodies impede lysosomal storage reduction during enzyme replacement therapy of a lysosomal storage disease. *J. Mol. Med.*, **86**, 433–442.
16. Schröder, S., Matthes, F., Hyden, P., Andersson, C., Fogh, J., Müller-Loennies, S., Braulke, T., Gieselmann, V. and Matzner, U. (2010) Site-specific analysis of N-linked oligosaccharides of recombinant lysosomal arylsulfatase A produced in different cell lines. *Glycobiology*, **20**, 248–259.
17. Klein, D., Yaghootfam, A., Matzner, U., Koch, B., Braulke, T. and Gieselmann, V. (2009) Mannose 6-phosphate receptor-dependent endocytosis of lysosomal enzymes is increased in sulfatide-storing kidney cells. *Biol. Chem.*, **390**, 41–48.
18. Pardridge, W.M. (1991) Transnasal and intraventricular delivery. In Pardridge, W.M. (ed.), *Peptide Drug Delivery to the Brain*. Raven Press, New York, pp. 99–122.
19. Hemsley, K.M., Luck, A.J., Crawley, A.C., Hassiotis, S., Beard, H., King, B., Rozek, T., Rozaklis, T., Fuller, M. and Hopwood, J.J. (2009) Examination of intravenous and intra-CSF protein delivery for treatment of neurological disease. *Eur. J. Neurosci.*, **29**, 1197–1214.
20. Hemsley, K.M., Norman, E.J., Crawley, A.C., Auclair, D., King, B., Fuller, M., Lang, D.L., Dean, C.J., Jolly, R.D. and Hopwood, J.J. (2009) Effect of cisternal sulfamidase delivery in MPS IIIA Huntaway dogs—a proof of principle study. *Mol. Genet. Metab.*, **98**, 383–392 [Epub 28 July 2009].
21. Kakkis, E., McEntee, M., Vogler, C., Le, S., Levy, B., Belichenko, P., Mobley, W., Dickson, P., Hanson, S. and Passage, M. (2004) Intrathecal enzyme replacement therapy reduces lysosomal storage in the brain and meninges of the canine model of MPS I. *Mol. Genet. Metab.*, **83**, 163–174.
22. Castaneda, J.A., Lim, M.J., Cooper, J.D. and Pearce, D.A. (2008) Immune system irregularities in lysosomal storage disorders. *Acta Neuropathol.*, **115**, 159–174.
23. D'Hooge, R., Hartmann, D., Manil, J., Colin, F., Gieselmann, V. and De Deyn, P.P. (1999) Neuromotor alterations and cerebellar deficits in aged arylsulfatase A-deficient transgenic mice. *Neurosci. Lett.*, **273**, 93–96.
24. Wittke, D., Hartmann, D., Gieselmann, V. and Lullmann-Rauch, R. (2004) Lysosomal sulfatide storage in the brain of arylsulfatase A-deficient mice: cellular alterations and topographic distribution. *Acta Neuropathol. (Berl.)*, **108**, 261–271.
25. Belverud, S., Mogilner, A. and Schulder, M. (2008) Intrathecal pumps. *Neurotherapeutics*, **5**, 114–122.
26. Paxinos, G. and Franklin, K.B.J. (2001) *The Mouse Brain in Stereotaxic Coordinates*, 2nd edn. Academic Press, San Diego, CA.
27. Matzner, U., Harzer, K., Learish, R.D., Barranger, J.A. and Gieselmann, V. (2000) Long-term expression and transfer of arylsulfatase A into brain of arylsulfatase A-deficient mice transplanted with bone marrow expressing the arylsulfatase A cDNA from a retroviral vector. *Gene Ther.*, **7**, 1250–1257.
28. Schierau, A., Dietz, F., Lange, H., Schestag, F., Parastar, A. and Gieselmann, V. (1999) Interaction of arylsulfatase A with UDP-N-acetylglucosamine:Lysosomal enzyme-N-acetylglucosamine-1-phosphotransferase. *J. Biol. Chem.*, **274**, 3651–3658.
29. Baum, H., Dodgson, K.S. and Spencer, B. (1959) The assay of aryl sulfatase A and B in human urine. *Clin. Chim. Acta*, **4**, 453–455.
30. Scott, J.E. and Dorling, J. (1965) Differential staining of acid glycosaminoglycans (mucopolysaccharides) by alcian blue in salt solutions. *Histochemistry*, **5**, 221–233.